INPOP new release: INPOP13c

A. Fienga[1,2], H. Manche[1], J. Laskar[1], M. Gastineau[1], and A. Verma[2]

[1]Astronomie et Systèmes Dynamiques, IMCCE-CNRS UMR8028, 77 Av. Denfert-Rochereau, 75014 Paris, France
[2]AstroGéo, Géoazur-CNRS UMR7329, Observatoire de la Cte d'Azur, 250 avenue A. Einstein, 06560 Valbonne, France

Abstract

Based on the use of MESSENGER radiotracking data in the construction of new Mercury ephemerides ([12]) a new planetary ephemerides INPOP13c was built including Mercury improvements but also improvements on the Mars orbit and on the tie of INPOP planetary ephemerides to ICRF in general.

1 INPOP13c

The MESSENGER mission was the first mission dedicated to the study on Mercury. The spacecraft orbits the smallest and the Sun closest planet of the solars system since 2011. ([12]) described the methods and procedures used for the analysis of the MESSENGER Doppler and range data included in the construction of the Mercury improved ephemerides, INPOP13a.

INPOP13c is an upgraded version of INPOP13a, fitted to LLR observations, and including new observations of Mars and Venus deduced from MEX, Mars Odyssey and VEX tracking ([9], [10] , [8]). The Pluto orbit was also improved with a better iterative procedure. Tables 7 and 8 resume the data samples and the obtained residuals with INPOP13c and INPOP10e common to the two ephemerides when Table 9 exhibits the residuals obtained for the data samples added since INPOP10e. Thanks to this supplementary material, a better extrapolation capability of the Mars ephemerides appears clearly in Tables 9, 4 and 5 as well as better consistencies between DE and INPOP ephemerides (see for example Table 2). The section 2 presents comparisons between INPOP13c, INPOP10e ([3]) and DE430 ([5]).

Adjustment of the gravitational mass of the sun was performed as recommended by the IAU resolution B2 as well as the sun oblateness (J_2), the ratio between the mass of the earth and the mass of the moon (EMRAT) and the mass of the Earth-Moon barycenter. Estimated values are presented on Table 1.

Masses of planets as well as procedures of estimations of the asteroid masses perturbing the inner planet orbits are the same as in INPOP10e and INPOP13a. Comparisons between asteroid masses obtained with INPOP13c and values gathered in [1] are given and discussed in section 3.

2 Estimation of uncertainties

Figures 1 to 8 present the differences in right ascension, declination and geocentric distances between INPOP13c, INPOP10e, DE430 and DE423 ([4]) over 120 years. The comparisons between INPOP13c

Table 1: Values of parameters obtained in the fit of INPOP13c, INPOP10e and DE430 to observations.

	INPOP13c $\pm 1\sigma$	INPOP10e $\pm 1\sigma$	DE430 $\pm 1\sigma$
(EMRAT-81.3000)$\times 10^{-4}$	(5.694 $\pm$ 0.010)	(5.700 $\pm$ 0.020)	($\pm$)
$J_2^{\odot} \times 10^{-7}$	(2.30 $\pm$ 0.25)	(1.80 $\pm$ 0.25)	1.80
$GM_{\odot}$ - 132712440000 [km^3. s^{-2}]	(44.487 $\pm$ 0.17)	(50.16 $\pm$ 1.3)	40.944
AU - 1.49597870700 $\times 10^{11}$ [m]	0.0	0.0	(-0.3738 $\pm$ 3)
[$M_{\odot}$ / M_{EMB}] - 328900	0.55314 $\pm$ 0.00033	0.55223 $\pm$ 0.004	0.55915 $\pm$ NC

Table 2: Maximum differences between INPOP13c, INPOP10e and DE430 from 1980 to 2020 in in α, δ and geocentric distances.

Geocentric Differences	INPOP13c - INPOP10e 1980-2020			INPOP13c - DE430 1980-2020			INPOP10e - DE423 1980-2020		
	α	δ	ρ	α	δ	ρ	α	δ	ρ
	mas	mas	km	mas	mas	km	mas	mas	km
Mercury	1.4	3.8	0.51	0.69	0.61	0.12	1.58	1.7	0.65
Venus	0.17	0.22	0.023	0.33	0.16	0.017	0.85	0.42	0.045
Mars	1.19	0.38	0.204	0.35	0.21	0.129	2.1	0.62	0.47
Jupiter	0.52	0.23	0.60	6.85	9.55	2.98	0.81	0.74	1.11
Saturn	0.24	0.72	0.25	0.75	0.49	1.72	0.82	0.53	1.82
Uranus	1.64	0.46	11.52	37.0	24.1	442.47	98.1	38.9	359.73
Neptune	24.4	9.65	1081	31.0	53.1	904.1	51.0	91.3	2054.8
Pluton	800.0	122.3	37384.1	112.0	39.8	465.4	703.2	152.7	37578.6

Table 3: Maximum differences between INPOP13c and other planetary ephemerides from 1980 to 2020 in cartesian coordinates of the earth in the BCRS.

Earth Barycentric Differences	XYZ	VxVyVz
	km	$mm.s^{-1}$
INPOP13c - INPOP10e	0.104	0.0177
INPOP13c - DE430	0.3763	0.0467
INPOP10e-DE423	0.84	0.113

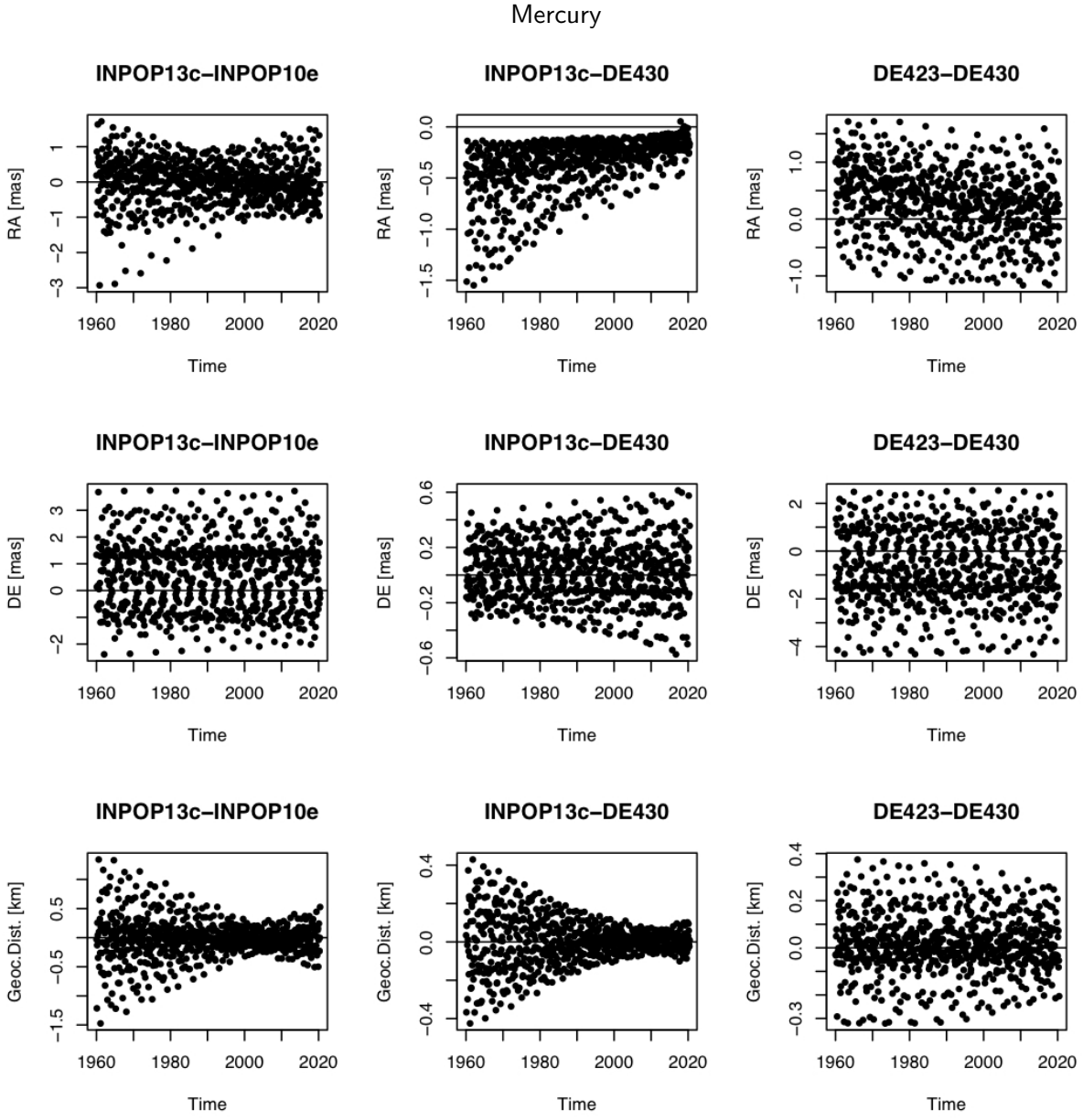

Figure 1: Differences in α, δ and geocentric distances between INPOP13c, INPOP10e, DE430 and DE423.

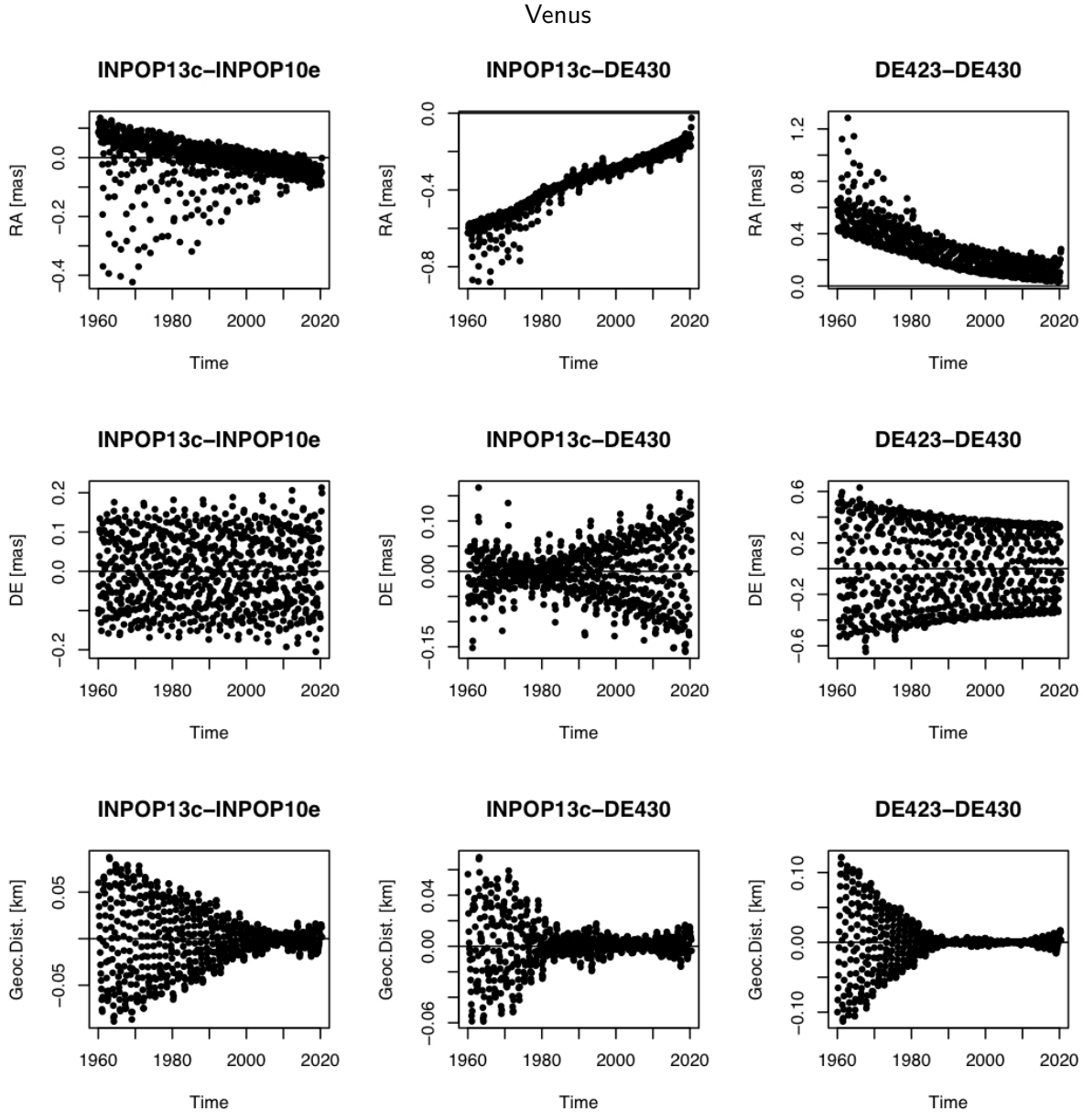

Figure 2: Differences in α, δ and geocentric distances between INPOP13c, INPOP10e, DE430 and DE423.

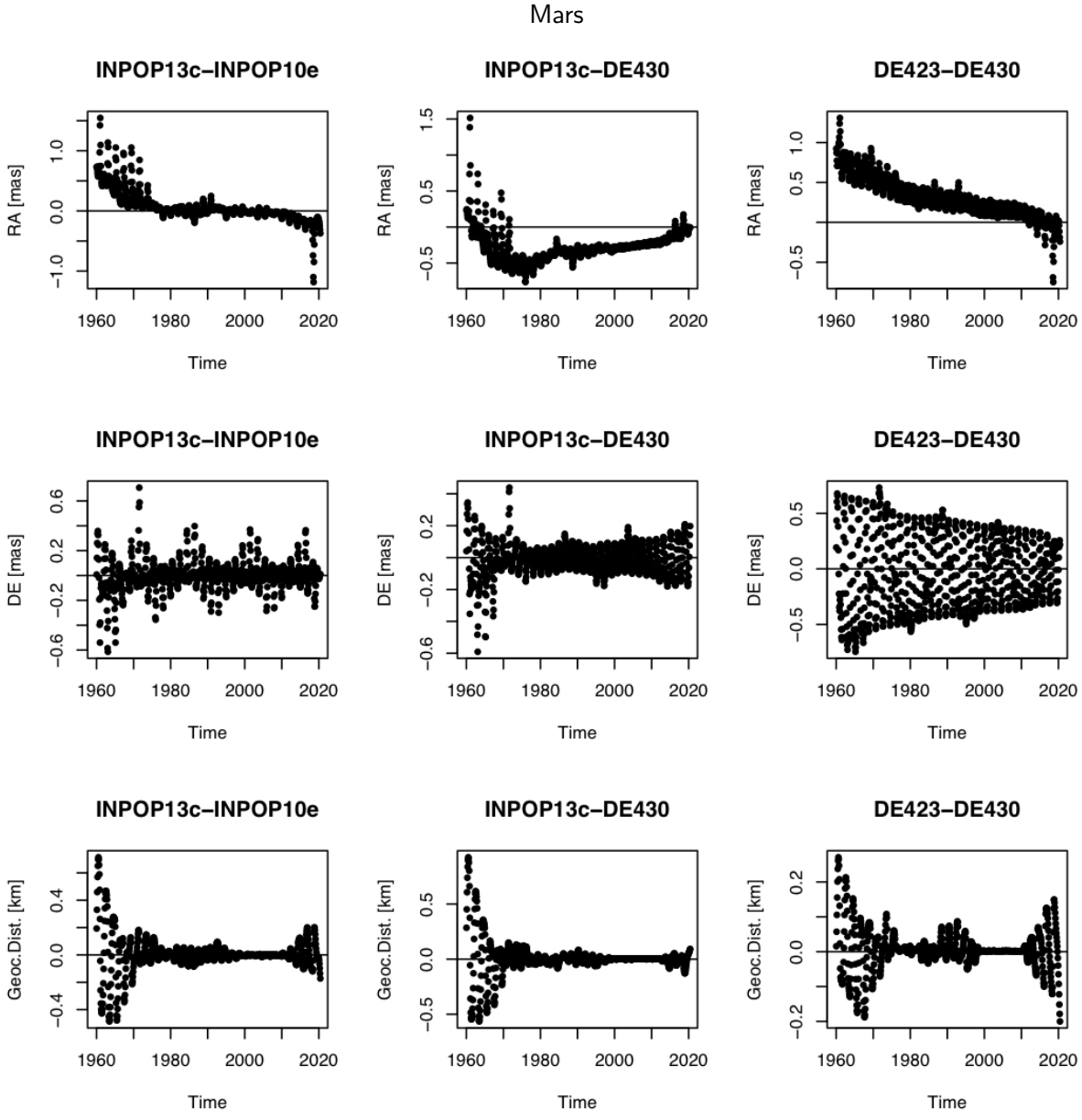

Figure 3: Differences in α, δ and geocentric distances between INPOP13c, INPOP10e, DE430 and DE423.

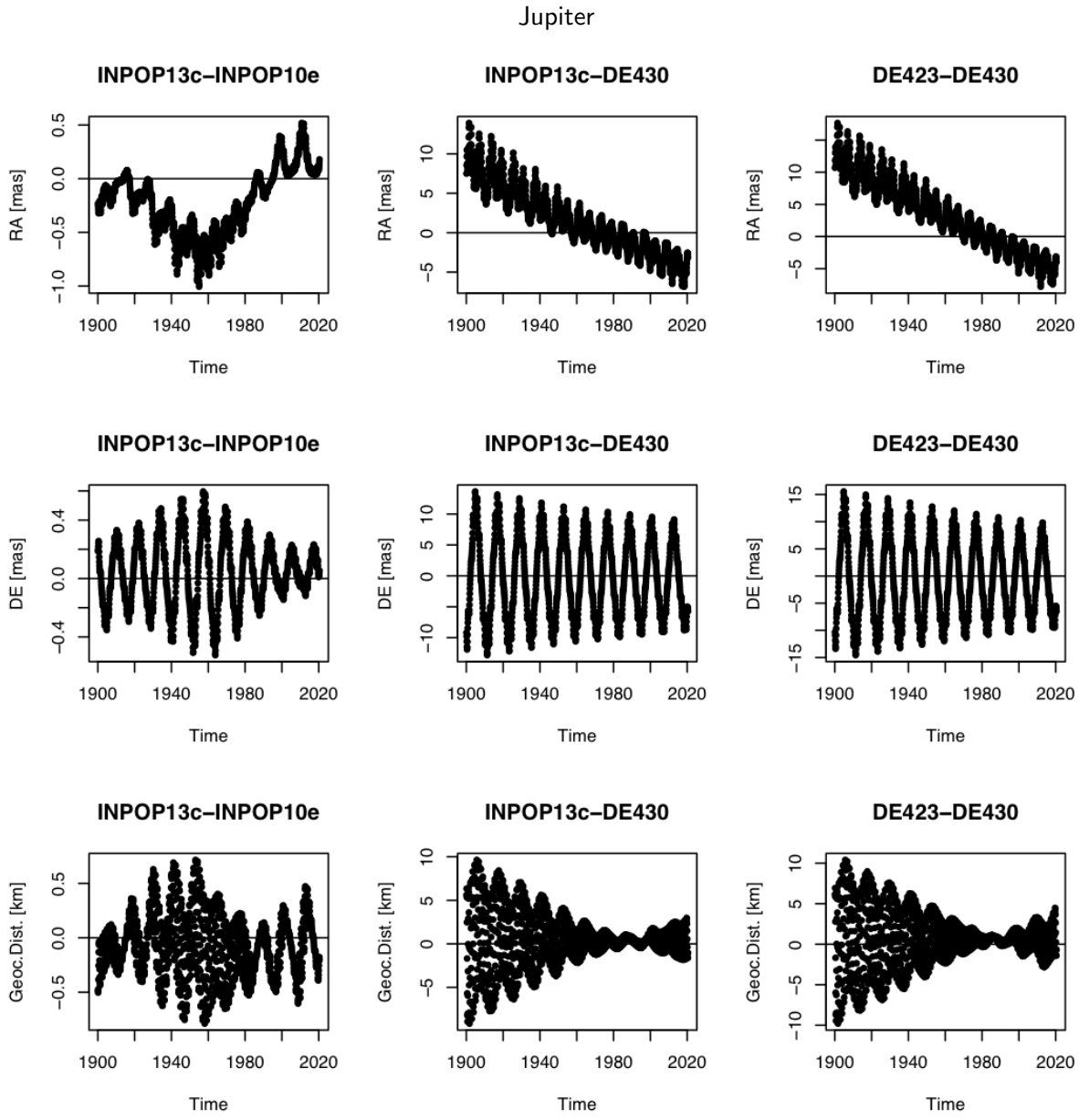

Figure 4: Differences in α, δ and geocentric distances between INPOP13c, INPOP10e, DE430 and DE423.

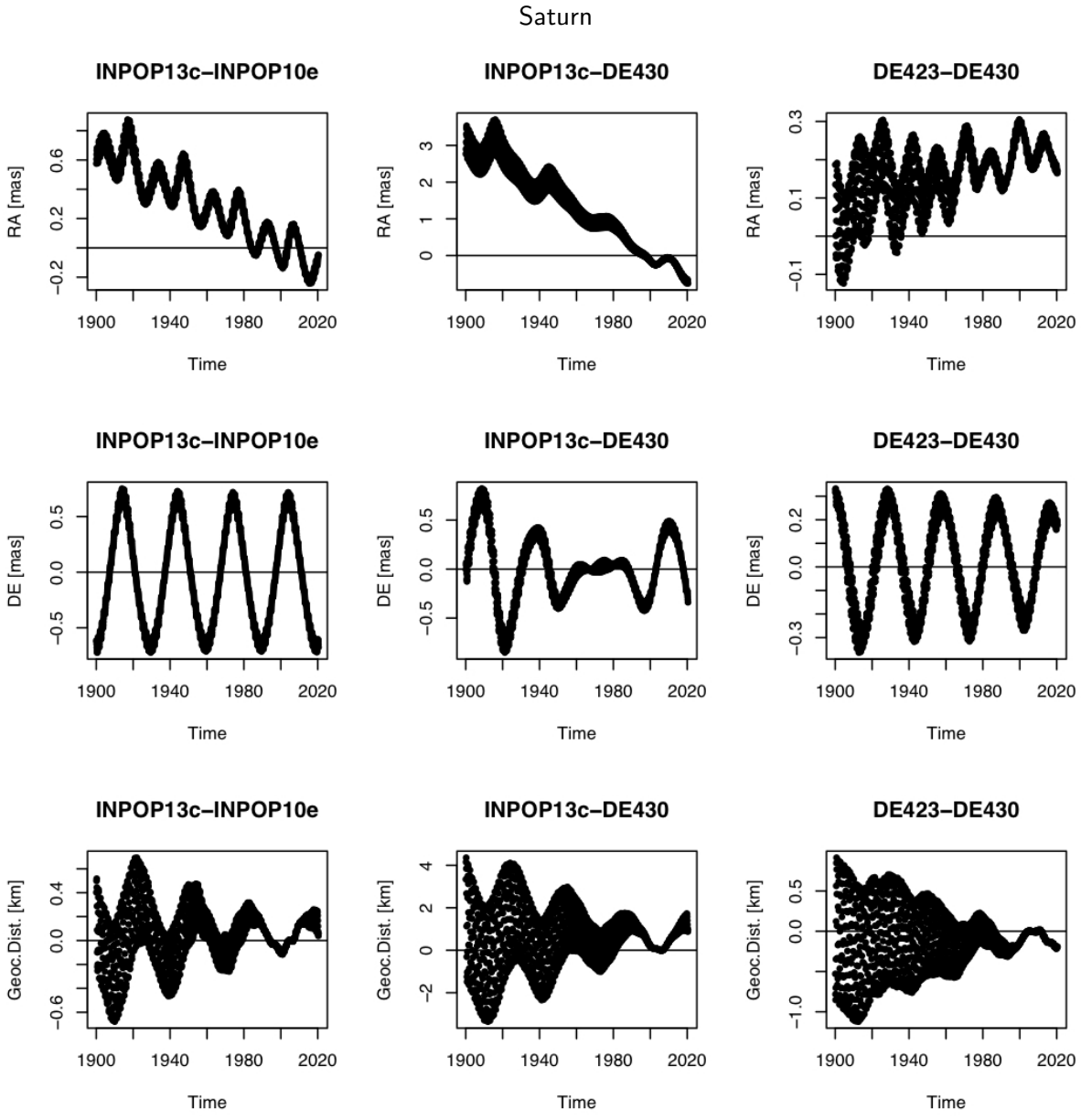

Figure 5: Differences in α, δ and geocentric distances between INPOP13c, INPOP10e, DE430 and DE423.

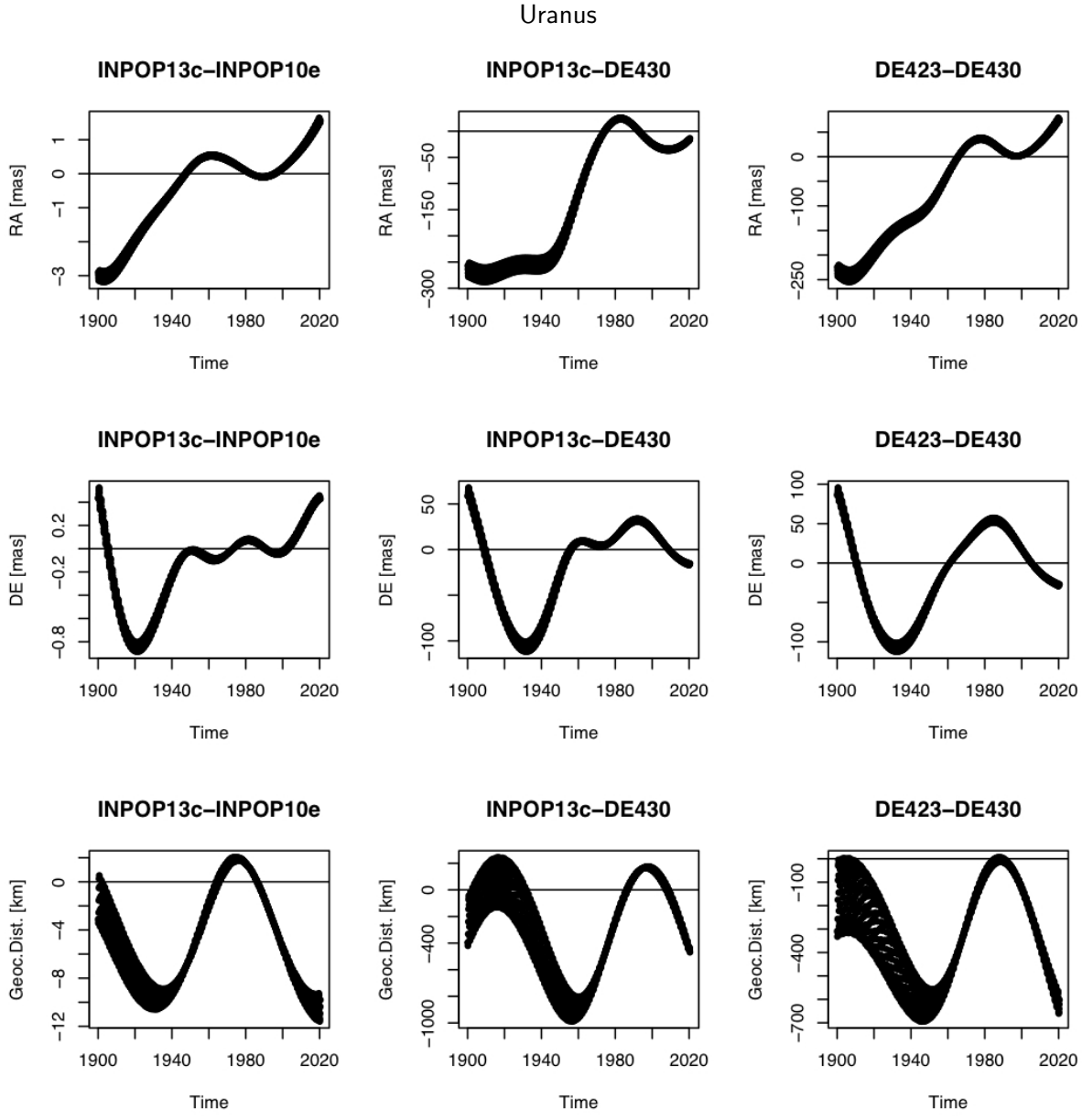

Figure 6: Differences in α, δ and geocentric distances between INPOP13c, INPOP10e, DE430 and DE423.

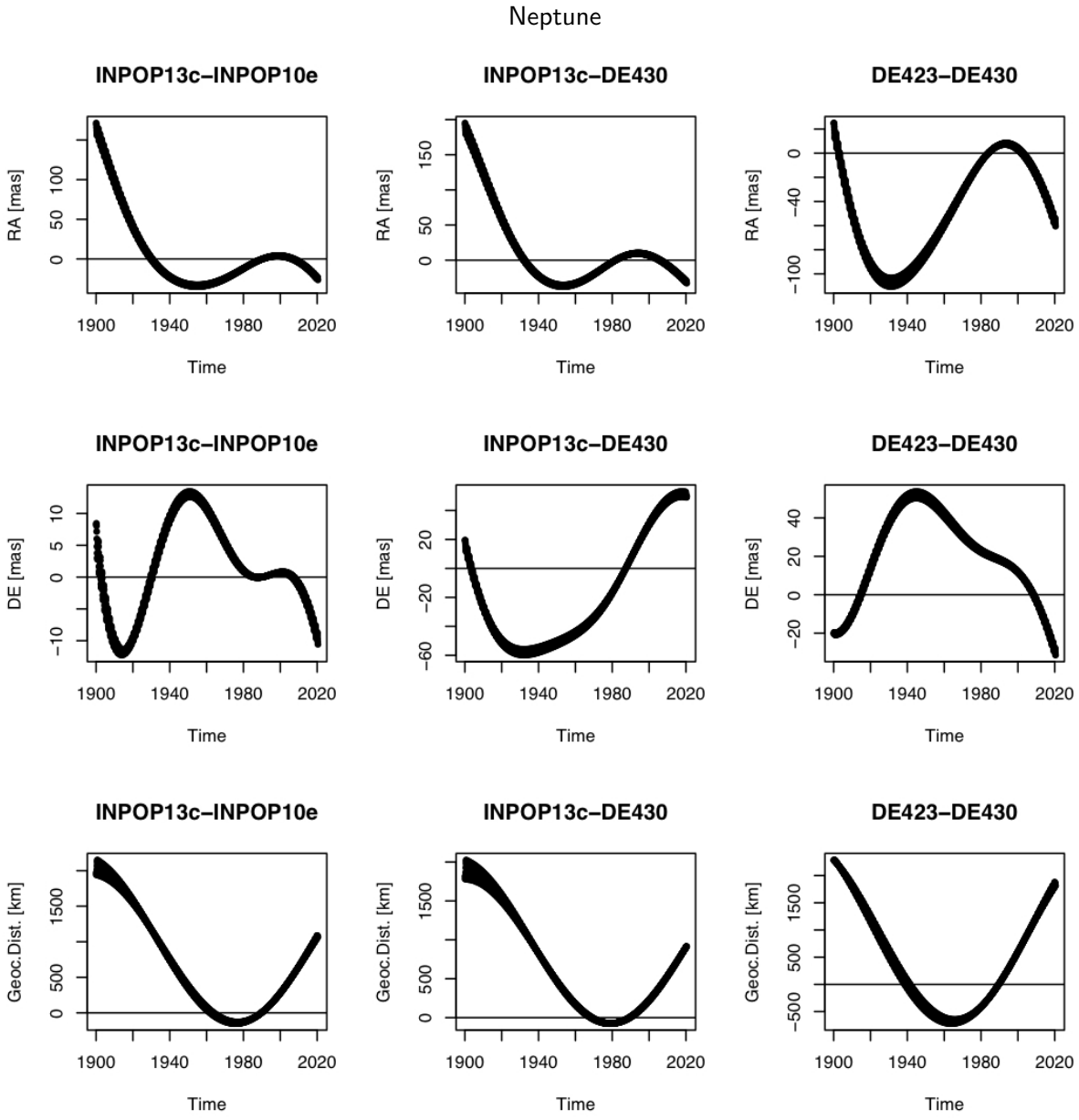

Figure 7: Differences in α, δ and geocentric distances between INPOP13c, INPOP10e, DE430 and DE423.

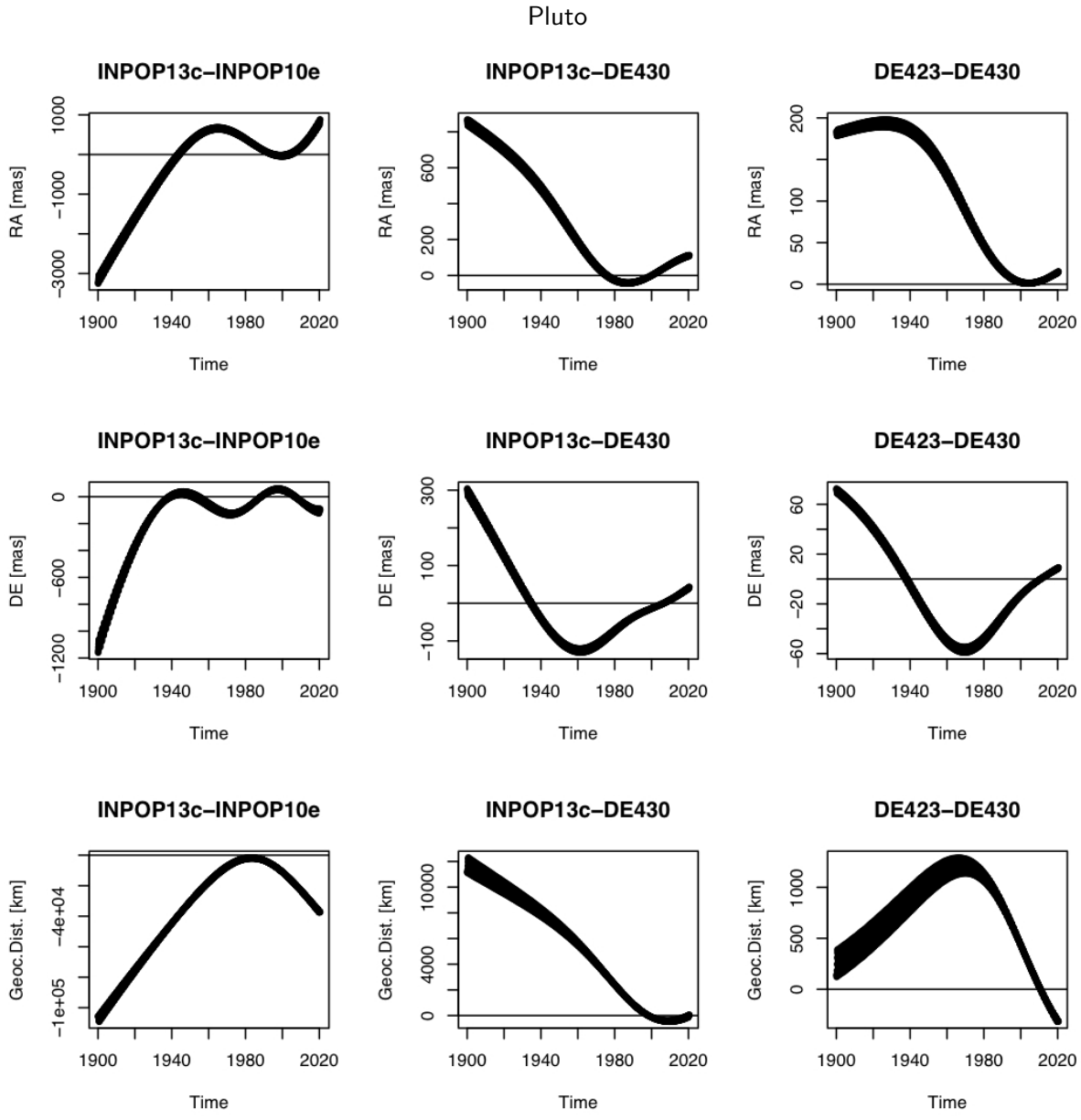

Figure 8: Differences in α, δ and geocentric distances between INPOP13c, INPOP10e, DE430 and DE423.

and INPOP10e show the improvement of INPOP13c due to the addition of new data samples. DE430 was fitted on about the same sample as INPOP13c except for Saturn Cassini normal points which were reprocessed (for more details see [5]). The comparisons between INPOP13c and DE430 give then an estimation of the ephemerides uncertainties induced by the use of different procedures of data analysis and of weighting schema. The differences DE430-DE423 are also plotted. The Tables 2 and 3 give the maximum differences obtained by comparisons between the same ephemerides on a 1980 to 2020 interval.

For the inner planets the differences pictured on Figures 1,2 and 3 show a good consistency between DE430, INPOP13c and INPOP10e.
For Mercury, the impact of the MESSENGER range bias used for INPOP13c and DE430 construction is clear on the post-2010 period. One can notice an increase of the differences in geocentric distances between INPOP13c and INPOP10e with the time. This increase does not appear in the DE423-DE430 differences. This fact could be explained by the lack of accurate observations before 2008 and the launch of MESSENGER. It is also noticed in the comparisons of the postfit residuals of Mariner data set in the Table 7. The Table 9 illustrates the improvement brought by the use of the MESSENGER range bias in the construction of INPOP13c by comparing INPOP13c postfit residuals and residuals obtained with INPOP10e. The one-order of magnitude improvement is consistent with INPOP13a ([12]) and is also illustrated on the Figures of the Table 5.

For Venus, one can note that the differences between DE423 and DE430 are one-order of magnitude larger than those between INPOP13c, INPOP10e and DE430 demonstrating an improvement of the accuracy of Venus orbit, especially through the computation of the geocentric distances. A common increase of the one-way range residuals of a factor 3 for INPOP13c and INPOP10 after 2010 shown on Table 9 and on plots of the Table 5 illustrates a confirmed degradation of the VEX transpondeur with time.

For Mars, as one can see on Figure 3 and on Table 2 the differences from one ephemeris to another one are quite equivalent for angles and geocentric distances. This illustrates the intensive works done in the past few years for improving the extrapolation capabilities of the ephemerides for the highly perturbed Mars orbit. The figures of the Tables 4 and 5 also show the improvement of the smoothness of the postfit residuals obtained with INPOP13c.

In terms of reference frame, the VLBI observations of Mars orbiters give the strongest link to ICRF2 as explained in [5]. As the INPOP13c-DE430 differences obtained for α and δ are below 0.5 mas and as the postfit residuals of INPOP13c VLBI Mars observations are also below 0.5 mas, the link of INPOP13c to ICRF2 is garenteed to at least 0.5 mas over the observational time interval (from 1989.13 to 2007.97) but also over the interval of ephemeris comparisons (from 1980 to 2020). Globally we can notice very small differences (< 1 mas) in angular geocentric quantities over 60 years for inner planets.

For the outer planets, differences are showed on Figures 4, 5, 6 and 7. A summary of the maximum differences is given on Table 2 and postfit residuals are presented on Tables 7 and 8.
The Jupiter differences show an non-negligeable discrepency between INPOP13c, INPOP10e and DE423 in one hand and DE430 in the other hand. This appears for all quantities (α,δ and geocentic distances) reaching about 15 mas in δ for DE423-DE430 and INPOP13c-DE430 over 1 century and about 10 mas over the contemporary interval (from 1980 to 2020). On the opposite, the maximum differences obtained by comparing INPOP13c to INPOP10e or INPOP10e to DE423 (see Table 2) do not present such offsets. These results could be explained by the change of weights used for the construction of the ephemerides. The uncertainties of the Jupiter modern observations were indeed not well estimated due to failures in the operational procedures (for example with the Galileo High Gain Antenna) or due to indirect measurements during flybys ([5]). One can then wait to have better

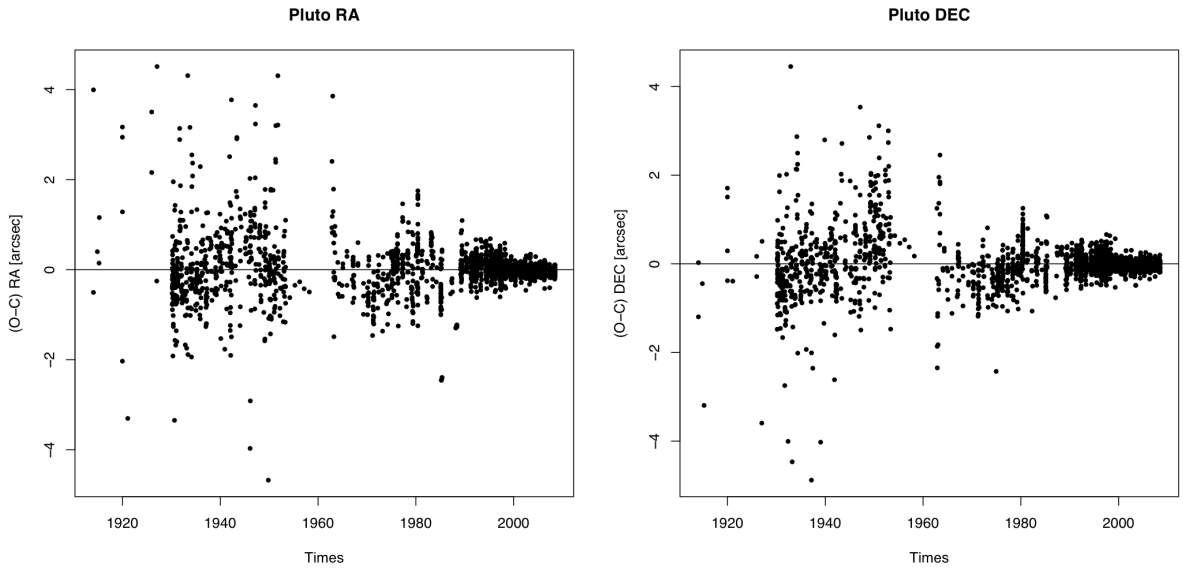

Figure 9: Pluto Postfit residuals in right ascension (RA) and declination (DE) in arcseconds obtained with INPOP13c.

inputs from the future Junon mission which is supposed to reach Jupiter in 2015.

Despite the use of new analysed Cassini tracking data in DE430, the differences of the Saturn orbits estimated with INPOP ephemerides and DE430 are less important than the Jupiter differences. They are also consistent with the expected accuracy of the observations used to constraint the orbit: angular differences are below 1 mas thanks to VLBI tracking of the Cassini spacecraft and differences in geocentric distances are about 1 km over the observational interval.

For Uranus and Neptune, the differences INPOP13c-DE430 and DE430-DE423 are compatible with the expected accuracy of the observations used for the construction of the ephemerides as given by the Table 2 maximum differences for the contemporary interval and by the postfit residuals of Table 8.

For Pluto, the large differences after 1960 pictured on Figure 8 and on Figure 2 are essentially induced by the important dispersions of photographic residuals used before the sixties for fitting the ephemerides. By the scanning of the photographic plates and by making a new analysis in using the future Gaia catalogue, one should be able to reduce drastically the noise of these data sets and then the uncertainties of the ephemerides for Pluto orbit. The arrival of the New Horizon spacecraft should help as well especially for the estimation of the size of the darwf planet's orbit. One can note however the good agreement of the ephemerides for the recent period thanks to the stellar occultation used for INPOP and DE constructions.

3 Asteroid masses

139 asteroids are used in INPOP13c with 87 asteroid masses actually estimated during the fit, 52 being fixed to masses derived from taxonomic classes and diameter estimations or to better mass estimations deduced from binary system or spacecraft flybys. No asteroid ring is considered in INPOP13c. Comparisons between the 87 asteroid masses obtained during the INPOP13c fit and

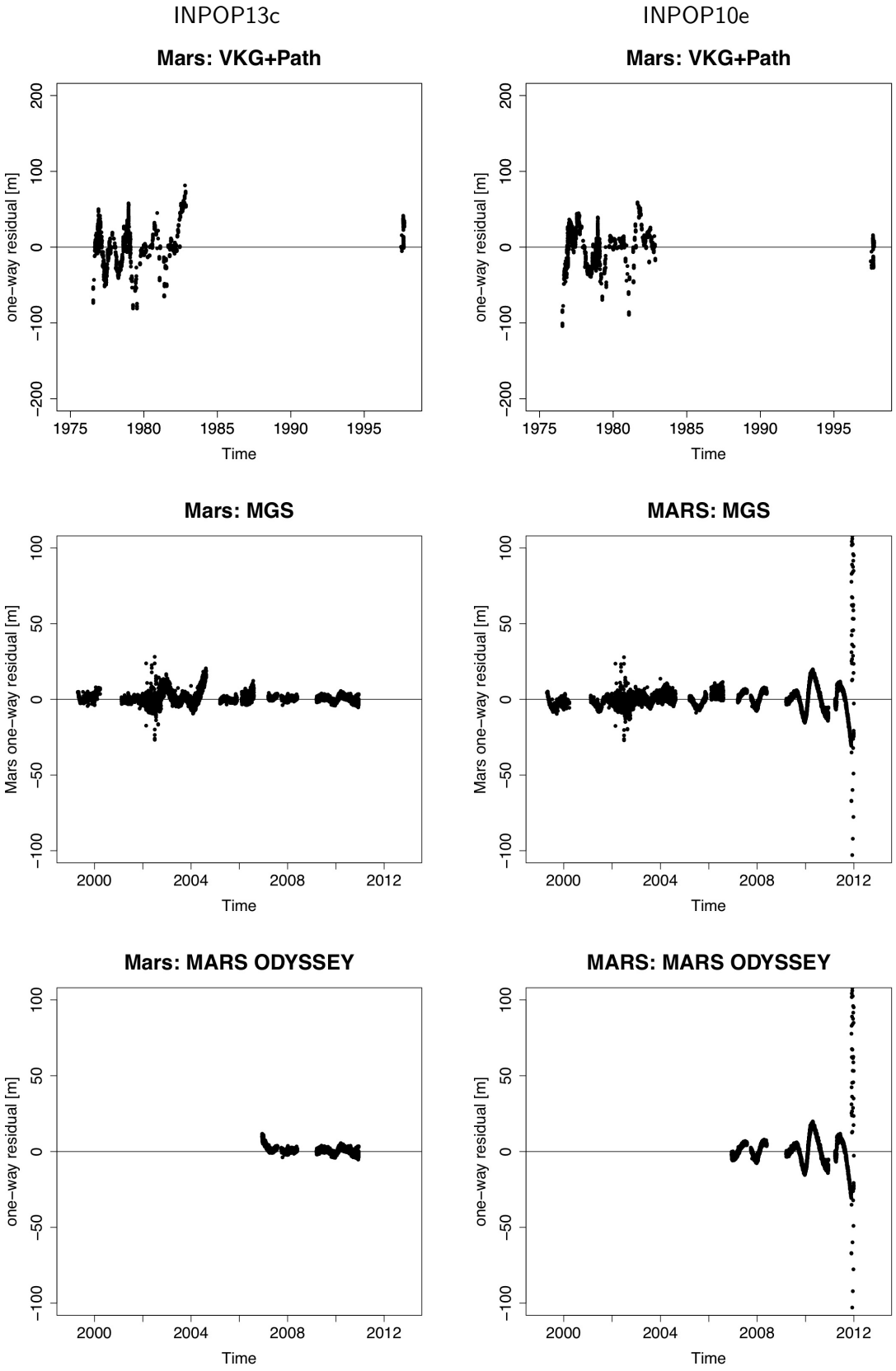

Table 4: Residuals for Mars Viking, Pathfinder, MGS and Mars Odyssey one-way range in meters obtained with INPOP10e, INPOP13c.

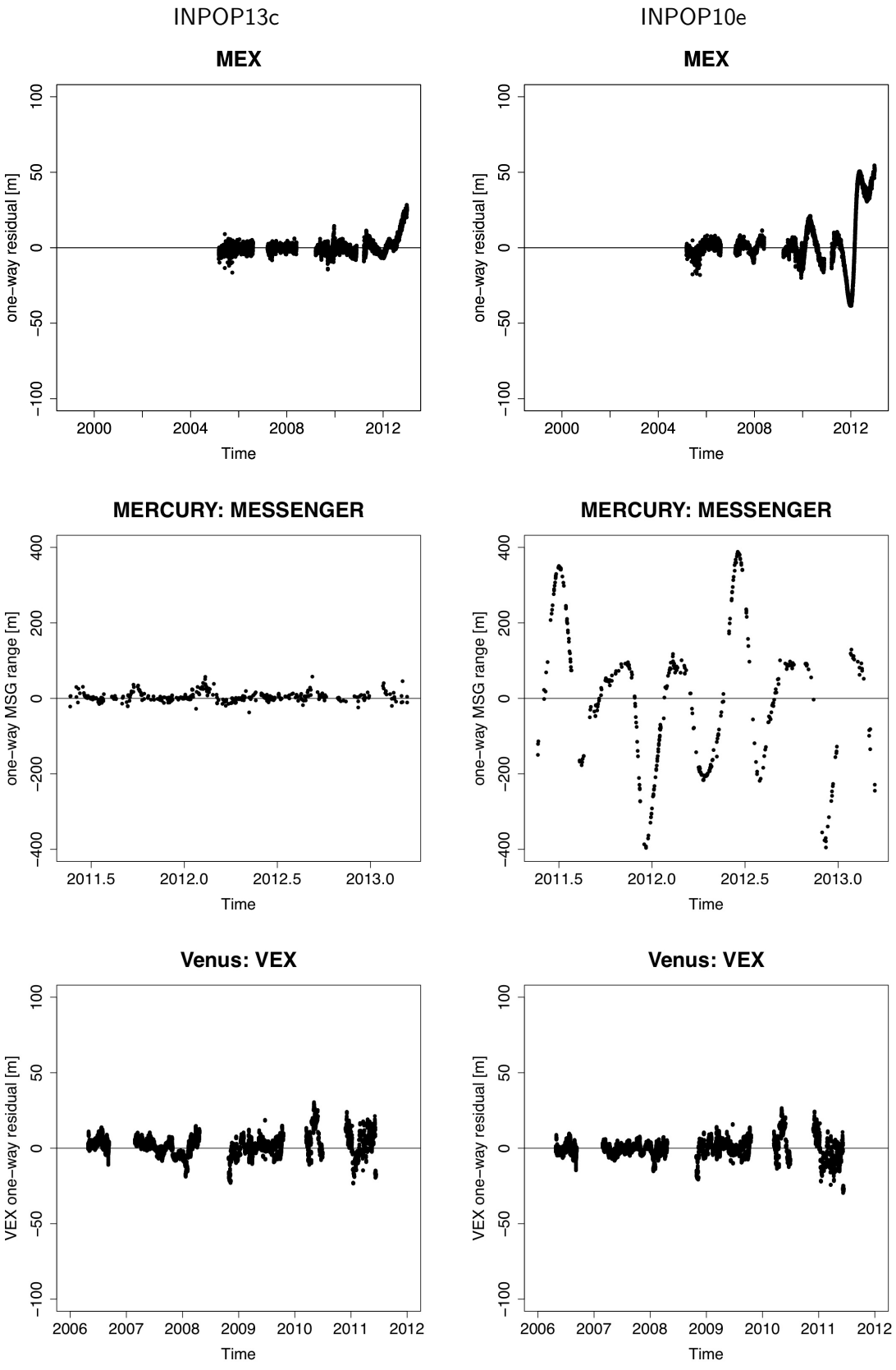

Table 5: Residuals for Mars MEX orbiter, Mercury MESSENGER and Venus VEX one-way range in meters obtained with INPOP13c and INPOP10e

masses collected by [1] are presented in Tables 10 and 11 and in Figure 10. Figure 10 pictures a log-log relation between asteroid masses and asteroid diameters as shown in [1] and [2]. Such a trend is a good tool for analyzing the quality of asteroid masses deduced from INPOP13c. One can first notice than asteroids having their masses deduced from planetary ephemerides have their diameters bigger than 50 kilometers. Only big objects can induce perturbations detectable thought inner planet observations.

Three families of asteroids are furthermore be considered on Figure 10: the big perturbers (in red) of the Earth-Mars distances inducing more than 10 meters on the geocentric distances of Mars over a 40-year interval (as defined in [7]), the asteroids inducing a modification between 5 to 10 meters of the geocentric distances of Mars over the same interval of time (in blue) and the small perturbers (in green) modifying the Earth-Mars distances by less than 5 meters. As it appears clearly on Figure 10, the estimations of the first two classes are quite compatible with the one obtained by [1] and follow generally well the trend with the diameters. The estimations of the smallest perturbers are, however, less compatible with the trend.

The 42 masses of the first two classes of asteroids are gathered in Table 10. They represent 48% of the whole sample of the estimated masses and can be used for computing mean values of C, S, B and M densities as defined in [2] and mean cumulated masses for each of these classes as the results given in Table 6. The comparison to [1] obtained for the same sample of 42 masses confirms the consistency of the two samples. The comparison to estimations published by [2] and obtained for a whole population of asteroids indicates that most of the perturbing objects belong to the C and S taxonomic classes when a lack of M-class objects seems to correspond to less perturbing objects (small or far from Mars).

4 Lunar Laser Ranging

INPOP13c is fitted to LLR observations from 1969 to 2013. Compared to INPOP10e, more than 700 observations from CERGA, 800 from Apollo and 50 from Matera have beed added in the fit. The number of parameters fitted is now 66 instead of 65 for INPOP10e:

- an offset for Apollo observations between december 2010 and april 2012 has been added
- because of its better significance (ratio between the fitted value and the formal error), the Moon's Love number h_2 is now fitted instead of Moon's coefficient of potential C_{30} (fixed to LP150Q value)

The values of all fitted parameters are given in Tables 12, 13 and 14. Their formal errors (1σ) come from the covariance matrix of the least square fit and can be much smaller than the physical uncertainties.

On table 15 and figure 11 are given the LLR residuals. The degradation on recent data was already noticed with INPOP10e, but it is amplified with INPOP13c. For Cerga, the residuals grow from 4 to 6 centimeters between before and after 2009. For Apollo, the standard deviation grows continuously from 5 to 7.6 centimeters between 2006 and 2013. These increases of residuals would vanish with the fit of the tectonic plate motion for the corresponding stations, but we think the problem comes from the dynamical model, with a lack that can be partly compensated by a change in station motion.

On table 16 is shown a comparison of residuals between INPOP13c and several JPL's solutions. JPL's residuals are here obtained by applying the same reduction process (model of light propagation) to the planetary and lunar motions of the corresponding JPL's solution. Only parameters involved

in the reduction (see tables 13 and 14) are refitted. Residuals computed here are then certainly different from the ones computed directly by the JPL. One can see for DE421 a small degradation on Apollo data (from 4.5 cm to 5.1 cm); this solution was released in 2008 and it is normal to observe such a degradation on data that were not available at this time, and thus not used to constrain the parameters. It should be stressed that DE421 residuals are better than the ones of INPOP13c (even on recent data); it thus demonstrates the better quality (extrapolation capabilities) of DE421 dynamical model. For DE430, residuals are improved relativ to the ones of DE421; the dynamical model is slightly different (Earth tides, degrees of Moon's and Earth's potential) and it is fitted to the latest data. The bad behaviour of INPOP13c compared to JPL's solutions is thus certainly due to a lack in the dynamical model (missing interaction?). The main difference between INPOP and JPL's solutions is the presence (since DE418) of a lunar liquid core interacting with the mantle. Its equations are given in [13, eqs. 6,7,8]:

$$\begin{cases} \frac{d}{dt} I_m \vec{\omega}_m + \vec{\omega}_m \wedge I_m \vec{\omega}_m = \vec{T}_g + \vec{T}_{cmb} \\ \frac{d}{dt} I_f \vec{\omega}_f + \vec{\omega}_m \wedge I_f \vec{\omega}_f = -\vec{T}_{cmb} \\ \vec{T}_{cmb} = K_\nu \left(\vec{\omega}_f - \vec{\omega}_m \right) + \left(C_f - A_f \right) \left(\tilde{z} \cdot \vec{\omega}_f \right) \left(\tilde{z} \wedge \vec{\omega}_f \right) \end{cases} \quad (1)$$

In these expressions,

- I_m and I_f are respectively the inertia matrices of the mantle and the fluid core
- $\vec{\omega}_m$ and $\vec{\omega}_f$ are the instant rotation vectors of the mantle and the fluid core
- $\vec{T}_g$ is the gravitational torque exerted by external bodies (Sun, Earth, ...)
- $\vec{T}_{cmb}$ is the torque due to interactions at core/mantle boundary
- A_f and C_f are the moments of inertia of the axisymetrical fluid core
- $\tilde{z}$ is the direction of the pole of the mantle
- K_ν is a friction coefficient at the core/mantle boundary

Analysis of DE431 residuals are then interesting. This solution, similar to DE430, is briefly described in [5] and [5]. In order to provide a long term solution (especially in the past), the friction torque at the lunar core/mantle boundary has been neglected ($K_\nu = 0$ in eq. 1). In table 16, one can see that its behaviour on recent data is the same as INPOP13c's one, with standard deviations of residuals increasing with time for both Apollo and Cerga; the values reached are often greater than with INPOP13c. This indicates that not only a lunar core is necessary, but also that the friction torque at the core/mantle boudary must not be neglicted.

INPOP13c does not take into account any lunar core yet, even if expressions 1 are already implemented in the equations of motions. The problem is that with fixed values of physical parameters (I_f, $C_f - A_f$ and K_ν) close to DE421, DE423 or DE430 ones, after fit of 69 other parameters (the 66 ones fitted in INPOP13c and the initial conditions of the core's instant vector of rotation), there is no significant improvement on residuals. This is why the Lunar core has not been activated for INPOP13c.

In conclusion, INPOP13c is not a solution as good as DE430 (or DE421) on LLR observations, even if it is improved compared to INPOP10e (fitted to more recent data). A work is still in progress in order to determine optimal values for the physical parameters of the Lunar core, certainly farther away from JPL's ones.

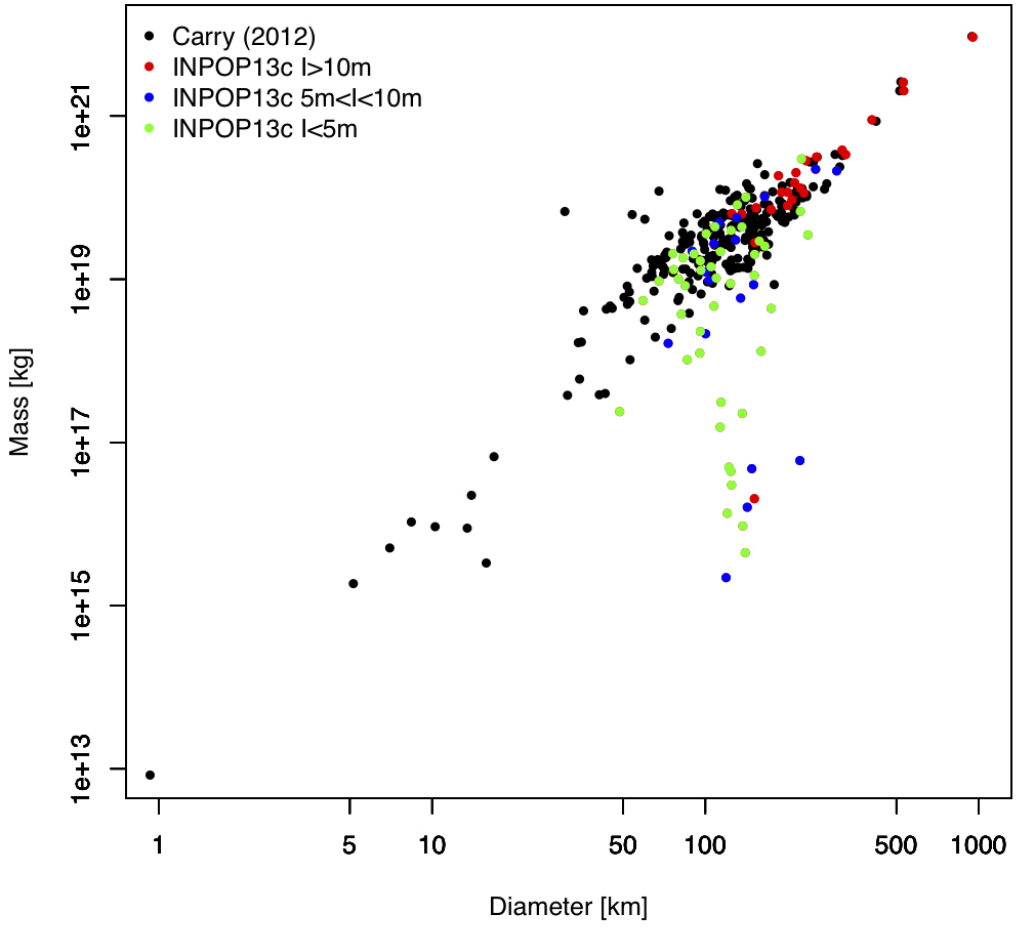

Figure 10: INPOP13c Asteroid mass determination. The x-axis is the log of diameters in kilometers (as given in [7]) when the y-axis is the log of the INPOP13c estimated masses in colors (see text) and of masses extracted from [1] in black. I stands for the impact in meters of the asteroids on the Earth-Mars distances over the interval from 1970 to 2010 (see [7]).

Table 6: Cumulated masses of the 42 most perturbing objects and deduced mean densities for taxonomic classes defined in [2].

	C-Class	S-Class	B-Class	M-Class	V-Class
This paper					
Cumulated mass [kg]	1.1973e+21	1.61e+20	2.04e+20	2.2e+19	2.590e+20
% of total mass	65%	9 %	11 %	1.2 %	14 %
% without CPVB	14 %	9 %	0 %	1.2%	0 %
Density [g.cm^{-3}]	2.19 $\pm$ 1.89	2.89 $\pm$ 1.79	2.59	2.40 $\pm$ 2.26	3.32
(DeMeo and Carry 2013)[2]					
Cumulated mass [kg]	1.42e+21	2.27e+20	3.0e+20	8.82+19	2.59e+20
% of total mass	52%	8.4 %	11.10 %	3.26 %	9.59 %
% without CPVB	14 %	8.4 %	3.5 %	3.26 %	0.01 %
Density [g.cm^{-3}]	1.33 $\pm$ 0.58	2.72 $\pm$ 0.54	2.38 $\pm$ 0.45	3.49 $\pm$ 1.00	1.93 $\pm$ 1.07
(Carry 2012)[1]					
Cumulated mass [kg]	1.18864e+21	1.5007e+20	2.04e+20	2.863e+19	2.63e+20
% of total mass	65%	8.2 %	11.10 %	1.56 %	14 %
% without CPVB	13%	8.2%	0 %	1.56%	0 %
Density [g.cm^{-3}]	1.54 $\pm$ 0.55	2.85 $\pm$ 1.04	2.30	4.53 $\pm$ 2.38	3.00

Table 7: Statistics of the residuals obtained after the INPOP13c fit for common data sample between INPOP13c and INPOP10e. For comparison, means and standard deviations of residuals obtained with INPOP10e.

Type of data		Nbr	Time Interval	INPOP10e		INPOP13c	
Mercury	range [m]	462	1971.29 - 1997.60	-45.3	872.499	-101.524	861.494
Mercury Mariner	range [m]	2	1974.24 - 1976.21	-31.850	109.191	-196.405	19.636
Mercury flybys Mess	ra [mas]	3	2008.03 - 2009.74	0.738	1.485	0.901	1.355
Mercury flybys Mess	de [mas]	3	2008.03 - 2009.74	2.422	2.517	2.472	2.408
Mercury flybys Mess	range [m]	3	2008.03 - 2009.74	-5.067	5.804	3.190	7.699
Venus	VLBI [mas]	46	1990.70 - 2010.86	1.590	2.602	1.591	2.575
Venus	range [m]	489	1965.96 - 1990.07	500.195	2234.924	504.569	2237.636
Venus Vex	range [m]	22145	2006.32 - 2009.78	-0.004	4.093	1.042	5.079
Mars	VLBI [mas]	96	1989.13 - 2007.97	-0.004	0.407	0.018	0.418
Mars Mex	range [m]	13842	2005.17 - 2009.78	0.485	3.189	-0.465	1.840
Mars MGS	range [m]	13091	1999.31 - 2006.83	-0.341	3.805	0.362	3.777
Mars Ody	range [m]	5664	2006.95 - 2010.00	0.280	4.155	1.55	2.30
Mars Path	range [m]	90	1997.51 - 1997.73	-6.289	13.663	19.324	14.096
Mars Vkg	range [m]	1257	1976.55 - 1982.87	-1.391	39.724	-1.494	41.189
Jupiter	VLBI [mas]	24	1996.54 - 1997.94	-0.291	11.068	-0.450	11.069
Jupiter	ra [arcsec]	6532	1914.54 - 2008.49	-0.039	0.297	-0.039	0.297
Jupiter	de [arcsec]	6394	1914.54 - 2008.49	-0.048	0.301	-0.048	0.301
Jupiter flybys	ra [mas]	5	1974.92 - 2001.00	2.368	3.171	2.554	2.961
Jupiter flybys	de [mas]	5	1974.92 - 2001.00	-10.825	11.497	-10.853	11.425
Jupiter flybys	range [m]	5	1974.92 - 2001.00	-907.0	1646.210	-985.957	1775.627
Saturne	ra [arcsec]	7971	1913.87 - 2008.34	-0.006	0.293	-0.006	0.293
Saturne	de [arcsec]	7945	1913.87 - 2008.34	-0.012	0.266	-0.012	0.266
Saturne VLBI Cass	ra [mas]	10	2004.69 - 2009.31	0.215	0.637	0.113	0.630
Saturne VLBI Cass	de [mas]	10	2004.69 - 2009.31	0.280	0.331	-0.115	0.331
Saturne Cassini	ra [mas]	31	2004.50 - 2007.00	0.790	3.879	0.663	3.883
Saturne Cassini	de [mas]	31	2004.50 - 2007.00	6.472	7.258	5.906	7.284
Saturne Cassini	range [m]	31	2004.50 - 2007.00	-0.013	18.844	0.082	23.763

Table 8: Statistics of the residuals obtained after the INPOP13c fit for common data sample between INPOP13c and INPOP10e. For comparison, means and standard deviations of residuals obtained with INPOP10e are given.

Type of data		Nbr	Time Interval	INPOP10e		INPOP13c	
Uranus	ra [arcsec]	13016	1914.52 - 2011.74	0.007	0.205	0.007	0.205
Uranus	de [arcsec]	13008	1914.52 - 2011.74	-0.006	0.234	-0.006	0.234
Uranus flybys	ra [arcsec]	1	1986.07 - 1986.07	-0.021	0.000	-0.021	0.000
Uranus flybys	de [arcsec]	1	1986.07 - 1986.07	-0.028	0.000	-0.028	0.000
Uranus flybys	range [m]	1	1986.07 - 1986.07	19.738	0.000	20.771	0.000
Neptune	ra [arcsec]	5395	1913.99 - 2007.88	0.000	0.258	0.003	0.258
Neptune	de [arcsec]	5375	1913.99 - 2007.88	-0.000	0.299	-0.002	0.299
Neptune flybys	ra [arcsec]	1	1989.65 - 1989.65	-0.012	0.000	-0.011	0.000
Neptune flybys	de [arcsec]	1	1989.65 - 1989.65	-0.005	0.000	-0.005	0.000
Neptune flybys	range [m]	1	1989.65 - 1989.65	69.582	0.000	51.507	0.000
Pluto	ra [arcsec]	2458	1914.06 - 2008.49	0.034	0.654	0.020	0.574
Pluto	de [arcsec]	2462	1914.06 - 2008.49	0.007	0.539	0.001	0.525
Pluto Occ	ra [arcsec]	13	2005.44 - 2009.64	0.003	0.047	-0.100	0.044
Pluto Occ	de [arcsec]	13	2005.44 - 2009.64	-0.006	0.018	0.000	0.027
Pluto HST	ra [arcsec]	5	1998.19 - 1998.20	-0.033	0.043	-0.018	0.044
Pluto HST	de [arcsec]	5	1998.19 - 1998.20	0.028	0.048	-0.026	0.048

Table 9: Statistics of INPOP13c postfit residuals for new samples included in the fit. For comparison, means and standard deviations of residuals obtained with INPOP10e on these prolongated intervals are also given.

Type of data		Nbr	Time Interval	INPOP10e		INPOP13c	
Mercure Messenger	range [m]	371	2011.39 - 2013.20	7.239	189.739	4.008	12.387
Venus Vex	range [m]	2825	2009.78 - 2011.45	1.84	16.54	5.12	15.70
Mars Mex	range [m]	12268	2009.78 - 2013.00	3.646	23.296	1.234	5.571
Mars Ody	range [m]	3510	2010.00 - 2012.00	4.834	9.586	0.741	1.778

Table 10: Asteroid masses obtained with INPOP13c and compared with values extracted from [1]. This table gathers the asteroids inducing a maximum change of more than 5 meters on the Earth-Mars distances on a [1970:2010] interval. Column 4 gives the value of this maximum impact of each asteroid on the Earth-Mars distances as defined in [7]. The Column 5 gives values of diameters obtained from IRAS and WISE surveys as given by [7] and Columns 6 and 7 present the masses and their uncertainties estimated by [1]. The last class gives the taxonomical index extracted from the Tholen classification ([11]).

IAU designation	INPOP13c	1-σ	Impact	diam	Carry 2012	1-σ	T-Class
	kg	kg	m	km	kg	kg	
4	2.590564e+20	1.157098e+18	1198.9530440	530.00	2.63e+20	5.00e+18	V
1	9.291844e+20	3.844558e+18	793.7412482	952.40	9.44e+20	6.00e+18	G
2	2.041335e+20	2.714066e+18	146.2695538	532.00	2.04e+20	4.00e+18	B
324	1.138045e+19	5.419632e+17	93.5357526	229.44	1.03e+19	1.00e+18	CP
10	8.980667e+19	7.853611e+18	77.0025537	407.12	8.63e+19	5.20e+18	C
19	8.003182e+18	9.346277e+17	59.0689816	200.00	8.60e+18	1.46e+18	G
3	2.834174e+19	1.300802e+18	55.6392528	233.92	2.73e+19	2.90e+18	S
704	3.821399e+19	4.131905e+18	34.4922565	316.62	3.28e+19	4.50e+18	F
532	1.310927e+19	1.512167e+18	32.7144140	222.39	1.15e+19	2.80e+18	S
9	1.165527e+19	1.205371e+18	29.6062727	190.00	8.39e+18	1.67e+18	S
7	1.162482e+19	9.666165e+17	27.8218292	199.83	1.29e+19	2.10e+18	S
29	1.517009e+19	1.903232e+18	26.6731763	212.22	1.29e+19	2.00e+18	S
13	9.372223e+18	2.364485e+18	22.0382227	207.64	8.82e+18	4.25e+18	G
15	3.149656e+19	1.569941e+18	21.5545880	255.33	3.14e+19	1.80e+18	S
6	1.855289e+19	1.282286e+18	21.1504947	185.18	1.39e+19	1.00e+18	S
14	2.813508e+18	9.790674e+17	18.1615646	152.00	2.91e+18	1.88e+18	S
11	7.499181e+18	1.387315e+18	17.3007697	153.33	5.91e+18	4.50e+17	S
8	6.288016e+18	7.000950e+17	12.6635308	135.89	9.17e+18	1.75e+18	S
45	2.021796e+19	2.393618e+18	11.7902641	214.63	5.79e+18	1.40e+17	FC
41	7.131347e+18	6.700157e+17	11.5682732	174.00	6.31e+18	1.10e+17	C
405	6.376346e+18	3.743249e+17	11.3784687	124.90	1.38e+18	1.40e+17	C
145	2.042610e+15	2.192145e+15	11.0486157	151.14	2.08e+18	5.70e+17	C
511	3.371614e+19	5.716552e+18	10.2480612	326.06	3.38e+19	1.02e+19	C
52	2.124138e+19	4.905582e+18	9.8407320	302.50	2.38e+19	5.80e+18	CF
16	2.229501e+19	3.642799e+18	9.7005515	253.16	2.72e+19	7.50e+18	M
419	3.030678e+18	9.012887e+17	9.5851372	129.01	1.72e+18	3.40e+17	F
23	2.730810e+18	5.714392e+17	9.0667512	107.53	1.96e+18	9.00e+16	S
488	8.576408e+17	3.383274e+18	8.6136830	150.13	2.48e+18	1.14e+18	C
230	4.342298e+18	1.927946e+18	7.6195204	108.99	1.89e+18	1.90e+17	S

IAU designation	INPOP13c	1-σ	Impact	diam	Carry 2012	1-σ	T-Class
	kg	kg	m	km	kg	kg	
187	5.686063e+18	7.819741e+17	7.5924498	130.40	1.80e+18	8.50e+17	C
111	5.869674e+17	1.980823e+18	6.9848015	134.55	1.76e+18	4.40e+17	C
109	2.209681e+18	5.165756e+17	6.8652431	89.44	NA	NA	GC
42	2.145282e+17	6.694597e+17	6.8289220	100.20	1.58e+18	5.20e+17	S
63	9.693634e+17	2.797805e+17	6.4510297	103.14	1.53e+18	1.50e+17	S
12	4.976460e+18	4.138827e+17	6.1587944	112.77	2.45e+18	4.60e+17	S
144	1.605988e+15	1.992285e+15	6.0865220	142.38	5.30e+18	1.20e+18	C
5	2.204297e+14	4.293857e+17	5.5329555	119.07	2.64e+18	4.40e+17	S
48	5.994443e+15	3.760429e+16	5.3602865	221.80	6.12e+18	2.96e+18	CG
59	1.025852e+19	3.278702e+16	5.3247597	164.80	3.00e+18	5.00e+17	CP
30	1.233848e+18	2.117636e+18	5.3223063	100.15	1.74e+18	4.90e+17	S
51	4.764145e+15	5.488586e+17	5.1088310	147.86	2.48e+18	8.60e+17	CU
516	1.638896e+17	7.806427e+17	5.0514023	73.10	1.43e+18	1.33e+18	M

References

[1] B. Carry. Asteroid masses. *Planetary and Space science*, 525:533–538, November 2012.

[2] F. E. DeMeo and B. Carry. The taxonomic distribution of asteroids from multi-filter all-sky photometric surveys. *Icarus*, 226:723–741, September 2013.

[3] A. Fienga, J. Laskar, H. Manche, M. Gastineau, and A. Verma. DPAC INPOP final release: INPOP10e. ArXiv e-prints , 2012.

[4] W. Folkner. Planetary ephemeris fit to Messenger encounters with Mercury. Technical report, JPL Interoffice Memorandum IOM 343.R-10-001, 2010.

[5] W. M. Folkner, J. G. Williams, D. H. Boggs, R. S. Park, and P. Kuchynka. The Planetary and Lunar Ephemerides DE430 and DE431. *Interplanetary Network Progress Report*, 196:C1, February 2014.

[6] A. S. Konopliv, S. W. Asmar, E. Carranza, W. L. Sjogren, and D. N. Yuan. Recent Gravity Models as a Result of the Lunar Prospector Mission. *Icarus*, 150:1–18, March 2001.

[7] P. Kuchynka, J. Laskar, A. Fienga, and H. Manche. A ring as a model of the main belt in planetary ephemerides. *A&A*, 514:A96+, May 2010.

[8] J.-C. Marty. Mars odyssey data release. Technical report, 2013. Private communication.

[9] T. Morley. MEX and VEX data release, 2012. Private communication.

[10] T. Morley. MEX and VEX data release, 2013. Private communication.

[11] D. J. Tholen. *Asteroid taxonomy from cluster analysis of Photometry.* PhD in astronomy, Arizona Univ., Tucson., 1984.

[12] A. K. Verma, A. Fienga, J. Laskar, H. Manche, and M. Gastineau. Use of MESSENGER radioscience data to improve planetary ephemeris and to test general relativity. *A&A*, 561:A115, January 2014.

[13] J. G. Williams. Lunar Core and Mantle. What Does LLR See? In *16th International Workshop on Laser Ranging*, October 2008.

Table 11: Asteroid masses obtained with INPOP13c and compared with values extracted from [1]. This table gathers more specifically the asteroids inducing a maximum change of less than 5 meters on the Earth-Mars distances on a [1970:2015] interval.

IAU designation	INPOP13c	1-σ	Impact	diam	Carry 2013	1-σ
	kg	kg	m	km	kg	kg
89	2.017804e+18	1.158577e+18	4.8149336	151.46	6.71e+18	1.82e+18
451	2.979651e+19	6.217767e+18	4.7418532	224.96	1.09e+19	5.30e+18
313	1.283921e+18	7.546575e+17	4.7044991	96.34	NA	NA
554	2.286580e+17	5.142521e+17	4.7036067	95.87	6.59e+17	6.60e+16
107	6.787732e+18	2.890148e+18	4.6303383	222.62	1.12e+19	3.00e+17
65	3.495611e+18	1.697773e+18	4.5364039	237.26	1.36e+19	3.10e+18
21	1.677741e+18	1.476184e+18	4.5269608	95.76	1.70e+18	1.00e+16
694	2.041762e+18	8.867518e+17	4.1874011	90.78	NA	NA
120	4.385643e+17	5.288536e+18	3.9064935	174.10	NA	NA
46	3.971305e+18	1.247291e+18	3.5594356	124.14	5.99e+18	5.00e+17
37	4.399527e+18	3.294685e+17	3.5514669	108.35	NA	NA
216	4.422420e+15	6.267640e+17	3.4827870	124.00	4.64e+18	2.00e+17
164	1.420331e+18	2.912094e+17	3.4332830	104.87	9.29e+17	7.76e+17
410	8.832544e+17	2.119148e+17	3.3882431	123.57	6.24e+18	3.00e+17
56	1.536408e+16	5.755360e+17	3.2535822	113.24	4.61e+18	0.00e+00
34	2.178007e+18	3.787477e+17	3.2274053	113.54	3.66e+18	3.00e+16
95	4.382951e+18	6.566998e+17	3.0162129	136.04	NA	NA
268	4.455482e+14	2.584680e+14	2.8481781	139.89	3.25e+18	2.26e+18
814	1.032312e+18	1.703245e+18	2.8300815	109.56	NA	NA
209	1.310480e+17	6.530118e+18	2.5293436	159.94	4.59e+18	7.42e+18
337	5.473158e+17	1.595918e+17	2.4044223	59.11	1.08e+18	1.60e+17
386	2.542494e+18	1.501009e+18	2.3365190	165.01	8.14e+18	1.58e+18
739	4.680385e+17	1.611940e+18	2.2048585	107.53	1.16e+18	1.07e+18
602	3.002039e+15	2.484931e+15	2.0856729	124.72	1.02e+19	5.00e+17
141	8.167383e+18	1.558767e+18	1.9991831	131.03	8.25e+18	5.77e+18
804	2.932829e+18	9.832968e+17	1.9193459	157.58	5.00e+18	1.78e+18
776	1.110207e+18	8.848554e+17	1.8941086	151.17	2.20e+18	2.71e+18
127	4.973809e+15	1.581185e+16	1.7862193	122.00	3.08e+18	1.35e+18
308	1.010230e+19	2.356410e+18	1.7849603	140.69	NA	NA
762	9.469866e+14	5.543771e+14	1.7827179	137.08	1.40e+18	1.00e+17
72	1.031184e+17	4.485403e+17	1.7669342	85.90	3.32e+18	8.49e+18
455	8.340879e+17	8.288418e+17	1.6642197	84.41	1.19e+18	1.20e+17
626	3.600162e+18	1.432526e+18	1.4705847	100.73	3.24e+18	1.30e+18
503	3.725514e+17	4.182849e+17	1.2278253	81.68	2.85e+18	3.40e+17
62	1.242051e+17	3.255760e+18	1.1981127	95.39	NA	NA
97	1.830943e+18	1.484500e+18	1.1452324	82.83	1.33e+18	1.30e+17
675	2.053879e+18	1.689563e+18	0.8847463	76.00	1.20e+19	2.40e+18
618	1.354581e+15	7.772176e+14	0.8620717	120.29	NA	NA
250	1.008119e+18	3.968719e+17	0.8082673	79.75	NA	NA
287	9.492653e+17	2.409003e+17	0.7241231	67.60	NA	NA
196	2.272704e+16	6.600523e+17	0.7131689	136.39	4.00e+18	1.53e+18

IAU designation	INPOP13c	1-σ	Impact	diam	Carry 2013	1-σ
	kg	kg	m	km	kg	kg
33	3.321441e+18	1.068539e+18	0.6208345	NA	6.20e+18	7.40e+17
196	2.272704e+16	1.207070e+15	0.7131689	136.39	4.00e+18	1.53e+18
779	1.311013e+18	3.501955e+17	0.5186778	76.62	NA	NA
388	3.106367e+16	5.365290e+16	0.4414599	114.17	NA	NA
204	2.385408e+16	8.976265e+16	0.2667205	48.57	6.00e+17	1.81e+18

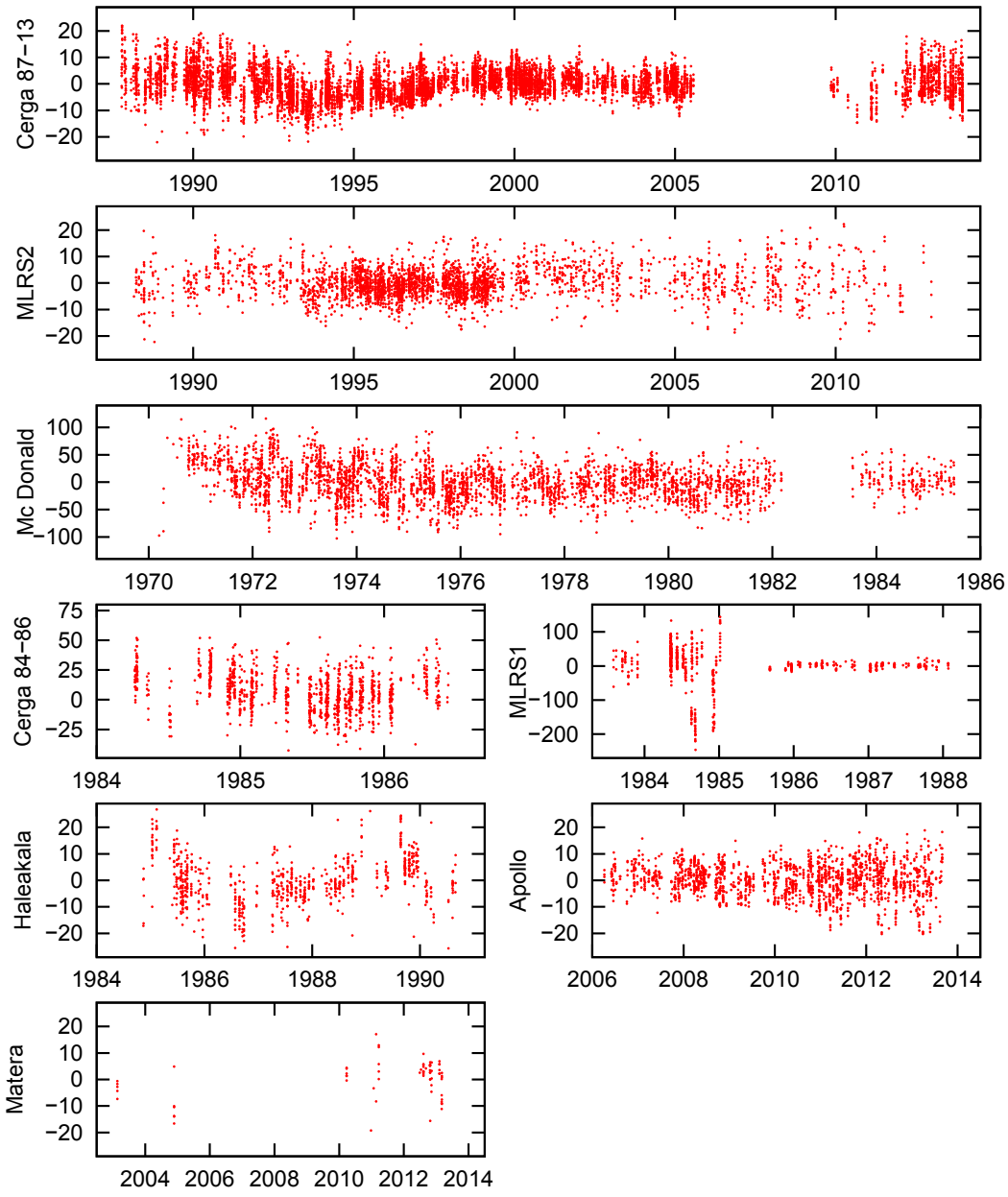

Figure 11: Postfit LLR residuals with INPOP13c for each station, expressed in centimeters.

Table 12: Values of dynamical parameters fitted to LLR observations. GM_{EMB} is the sum of Earth's and Moon's masses, multiplied by the gravitationnal constant and is expressed in AU^3/day^2. C_{nmE} are the Earth's coefficients of potential (without unit). τ_{21E} and τ_{22E} are time delays of the Earth used for tides effects and expressed in days. C_{nmM} and S_{nmM} are the Moon's coefficients of potential (without unit). $(C/MR^2)_M$ is the ratio between the third moment of inertia of the Moon, divided by its mass and the square of the mean equatorial radius (without unit). k_{2M} and τ_M are the Love number (without unit) and the time delay (in day) of the Moon. Formal errors at 1σ are given if the parameter is fitted and correspond to the values provided by the covariance matrix of the least square fit; one can note that the real uncertainties on parameters are generally much higher. Fixed values come from Lunar gravity model LP150Q [6] and Earth's ones from EGM96 (`cddis.nasa.gov/926/egm96`).

Name	Value	Formal error (1σ)
GM_{EMB}	$8.9970115728 \times 10^{-10}$	$\pm 9.0 \times 10^{-19}$
C_{20E}	$-1.0826225 \times 10^{-3}$	$\pm 1.0 \times 10^{-9}$
C_{30E}	2.756×10^{-6}	$\pm 3.7 \times 10^{-8}$
C_{40E}	$1.6196215913670001 \times 10^{-6}$	
τ_{21E}	1.239×10^{-2}	$\pm 8.1 \times 10^{-5}$
τ_{22E}	6.9768×10^{-3}	$\pm 6.7 \times 10^{-6}$
C_{20M}	-2.03377×10^{-4}	$\pm 1.8 \times 10^{-8}$
C_{22M}	2.23909×10^{-5}	$\pm 1.5 \times 10^{-9}$
C_{30M}	$-8.4745310957091 \times 10^{-6}$	
C_{31M}	3.154×10^{-5}	$\pm 3.6 \times 10^{-7}$
C_{32M}	$4.8452131769807101 \times 10^{-6}$	
C_{33M}	1.7198×10^{-6}	$\pm 5.9 \times 10^{-9}$
C_{40M}	$9.6422863508400007 \times 10^{-6}$	
C_{41M}	$-5.6926874002713197 \times 10^{-6}$	
C_{42M}	$-1.5861997682583101 \times 10^{-6}$	
C_{43M}	$-8.1204110561427604 \times 10^{-8}$	
C_{44M}	$-1.2739414703200301 \times 10^{-7}$	
S_{31M}	3.203×10^{-6}	$\pm 7.3 \times 10^{-8}$
S_{32M}	1.68738×10^{-6}	$\pm 4.9 \times 10^{-10}$
S_{33M}	$-2.4855254931699199 \times 10^{-7}$	
S_{41M}	$1.5743934836970999 \times 10^{-6}$	
S_{42M}	$-1.5173124037059000 \times 10^{-6}$	
S_{43M}	$-8.0279066452763596 \times 10^{-7}$	
S_{44M}	$8.3147478750240001 \times 10^{-8}$	
$(C/MR^2)_M$	3.93018×10^{-1}	$\pm 2.6 \times 10^{-5}$
k_{2M}	2.626×10^{-2}	$\pm 1.7 \times 10^{-4}$
τ_M	1.912×10^{-1}	$\pm 1.2 \times 10^{-3}$

Table 13: Selenocentric coordinates of reflectors (expressed in meters) and Moon's Love number h_2 (without unit).

Reflector		Value	Formal error (1σ)
Apollo XI	x	1591924.511	± 1.260
	y	690802.582	± 2.890
	z	21003.774	± 0.047
Apollo XIV	x	1652725.840	± 1.430
	y	-520890.307	± 2.010
	z	-109730.480	± 0.105
Apollo XV	x	1554674.570	± 0.963
	y	98196.294	± 3.000
	z	765005.696	± 0.048
Lunakhod 1	x	1114345.496	± 0.226
	y	-781226.597	± 2.820
	z	1076059.335	± 0.083
Lunakhod 2	x	1339314.148	± 1.460
	y	801958.776	± 2.430
	z	756359.229	± 0.083
Love number h_2		5.26×10^{-2}	$\pm 2.4 \times 10^{-3}$

Table 14: ITRF coordinates of stations at J1997.0, expressed in meters.

Station		Value	Formal error (1σ)
Cerga	x	4581692.122	± 0.003
	y	556196.023	± 0.001
	z	4389355.021	± 0.010
Mc Donald	x	-1330781.424	± 0.011
	y	-5328755.458	± 0.009
	z	3235697.527	± 0.021
MLRS1	x	-1330121.107	± 0.013
	y	-5328532.265	± 0.008
	z	3236146.619	± 0.022
MLRS2	x	-1330021.436	± 0.002
	y	-5328403.283	± 0.003
	z	3236481.629	± 0.010
Haleakala (rec.)	x	-5466000.412	± 0.011
	y	-2404424.718	± 0.014
	z	2242206.742	± 0.028
Apollo	x	-1463998.829	± 0.003
	y	-5166632.678	± 0.003
	z	3435013.069	± 0.010
Matera	x	4641978.858	± 0.018
	y	1393067.435	± 0.027
	z	4133249.634	± 0.036

Table 15: Means and standard deviations (both expressed in centimeters) of LLR residuals for INPOP13c solution. Na is the total number of observations available, Nk is the number kept in fitting process, Nr is the number that have been rejected according to the 3σ criterion (Na is always Nk+Nr).

Station	Period	Mean	Std. dev.	Na	Nk	Nr
Cerga	1984-1986	6.96	16.02	1188	1161	27
Cerga	1987-1995	-0.58	6.58	3443	3411	32
Cerga	1995-2006	0.06	3.97	4881	4845	36
Cerga	2009-2013	0.08	6.08	999	990	9
Mc Donald	1969-1983	-0.23	31.86	3410	3302	108
Mc Donald	1983-1986	4.02	20.60	194	182	12
MLRS1	1983-1984	5.92	29.43	44	44	0
MLRS1	1984-1985	-7.25	77.25	368	358	10
MLRS1	1985-1988	0.10	7.79	219	207	12
MLRS2	1988-1996	-0.43	5.36	1199	1166	33
MLRS2	1996-2012	0.15	5.81	2454	1972	482
Haleakala	1984-1990	-0.38	8.63	770	739	31
Apollo	2006-2010	0.25	4.92	941	940	1
Apollo	2010-2012	0.00	6.61	514	414	10
Apollo	2012-2013	-0.62	7.62	359	359	0
Matera	2003-2013	0.13	7.05	83	70	13

Table 16: Comparison of residuals (in cm) between INPOP13c, DE421, DE430 and DE431. For the JPL's solutions, the residuals are obtained by applying the same reduction model as INPOP13c to planetary and lunar motions from DExxx solutions, with all parameters of tables 13 and 14 refitted.

Station	Period	INPOP13c	DE421	DE430	DE431
Cerga	1984-1986	16.02	14.56	14.55	14.19
Cerga	1987-1995	6.58	5.87	5.64	6.27
Cerga	1995-2006	3.97	3.97	3.96	4.91
Cerga	2009-2013	6.08	3.84	3.52	6.94
Mc Donald	1969-1983	31.86	30.38	30.15	30.43
Mc Donald	1983-1986	20.60	19.54	19.83	19.58
MLRS1	1983-1984	29.43	27.86	27.68	28.02
MLRS1	1984-1985	77.25	73.80	72.70	73.85
MLRS1	1985-1988	7.79	5.54	5.45	5.96
MLRS2	1988-1996	5.36	5.16	4.88	5.49
MLRS2	1996-2012	5.81	4.93	4.94	5.97
Haleakala	1984-1990	8.63	8.59	8.33	8.76
Apollo	2006-2010	4.92	4.47	4.15	6.02
Apollo	2010-2012	6.61	4.99	4.31	7.85
Apollo	2012-2013	7.62	5.09	4.43	8.95
Matera	2003-2013	7.05	5.21	5.76	7.21